

Adhesion-induced phase behavior of multicomponent membranes

Thomas R. Weikl* and Reinhard Lipowsky

Max-Planck-Institut für Kolloid- und Grenzflächenforschung, 14424 Potsdam, Germany

(Received 27 July 2000; revised manuscript received 22 January 2001; published 13 June 2001)

Biomimetic membranes that contain several molecular components are studied theoretically. In contact with another surface, such as a solid substrate or another membrane, some of these intramembrane components are attracted by the second surface and, thus, act as local stickers. The *cooperative* behavior of these systems is characterized by the interplay of (i) attractive binding energies, (ii) entropic contributions arising from the shape fluctuations of the membranes, and (iii) the entropy of mixing of the stickers. A *systematic* study of this interplay, which starts from the corresponding partition functions, reveals that there are several *distinct* mechanisms for adhesion-induced phase separation within the membranes. The first of these mechanisms is effective for flexible stickers with attractive cis interactions (within the same membrane) and arises from the renormalization of these interactions by the confined membrane fluctuations. A second, purely entropic mechanism is found for rigid stickers without attractive cis interactions and arises from a fluctuation-induced line tension. Finally, a third mechanism is present if the membrane contains both stickers and repellers, i.e., nonadhesive molecules that protrude from the membrane surface. This third mechanism is based on an effective potential barrier and becomes less effective if the shape fluctuations of the membrane become more pronounced.

DOI: 10.1103/PhysRevE.64.011903

PACS number(s): 87.16.Dg, 05.70.Np, 05.10.Ln

I. INTRODUCTION

The adhesion of membranes is governed by a variety of generic and specific interactions that have been studied for some time [1]. In the simplest case, the membrane is composed of a lipid bilayer and has a homogeneous and uniform lateral composition. If such a membrane is in contact with a substrate surface or another membrane, it usually experiences a variety of molecular forces such as, e.g., van der Waals and/or electrostatic interactions. In addition, the confined membrane undergoes thermally excited shape fluctuations that can be directly observed using optical microscopy [2] and which act to renormalize the molecular force potentials [3].

Lipid bilayers represent the basic building blocks of cell membranes. These latter membranes also contain many different protein components. If such a multicomponent membrane is brought into contact with a second surface, this surface will act as a sorting agent since it attracts some membrane components but repels others. This interplay of adhesion and composition represents an interesting physical problem that will be considered here in the context of biomimetic membranes consisting of a few lipid components together with some anchored macromolecules. These macromolecules, which protrude from the membrane surface, act as local stickers or repellers if they experience attractive or repulsive interactions with the second surface, respectively. Stickers that are laterally mobile within the membrane will be recruited by the adhesive surface, and thus, have a tendency to be enriched within the contact area, whereas mobile repellers will become depleted within the same area.

Presumably the first theoretical models for the adhesion of membranes via mobile stickers were introduced in Refs.

[4,5] as reviewed in Ref. [6]. In these models, the membrane is divided into one bound segment, which represents the contact area, and one unbound segment, which acts as a sticker reservoir. The repellers are taken to be more or less immobile and the separation of the two interacting surfaces is taken to be constant within the contact area. In general, the competing action of stickers and repellers should lead to a modulation of this separation: sticker-rich membrane segments should have a relatively small separation, whereas repeller-rich segments should have a relatively large one as discussed in the context of gap junctions [7–9].

A systematic theoretical framework for the interplay of membrane adhesion and membrane composition was introduced in Ref. [10]. Within this framework, the membrane is divided into small membrane segments (or patches). The lateral size of these segments corresponds to the smallest possible wavelength for bending deformations of the membrane. Computer simulations for molecular membrane models indicate that this size is about 6 nm for lipid bilayers with a thickness of about 4 nm [11]. The configurational energy of each segment has two contributions: one contribution arising from the elastic deformation and another one from the interactions with the second surface. These interactions depend on the presence or absence of a sticker or repeller molecule within this segment. The configurational energy of the whole membrane is obtained by a summation over all membrane segments. In this way, one arrives at partition functions for lattice gas models on deformable membrane surfaces [10].

In general, the interplay of membrane adhesion and composition represents a cooperative process which depends on several free energy contributions: (i) attractive trans-interactions between the stickers and the adhesive surface characterized by the corresponding sticker/surface binding energy; (ii) entropic contributions arising from the shape fluctuations of the membrane that are governed by the ratio of membrane rigidity and temperature; (iii) attractive cis interactions between two stickers within the same membrane

*Present address: Department of Pharmaceutical Chemistry, University of California, San Francisco, CA 94143-1204.

that depend on the sticker/sticker binding energy; and (iv) the entropy of mixing arising from the mobility of the stickers within the membranes. In addition, the stickers may locally change the elastic properties of the membranes, an effect that will depend on the sticker size and on the sticker anchoring.

In the present article, we study the competition of these different contributions in a *systematic* way using the theoretical methods of statistical mechanics. Thus, we start from partition functions that include both shape fluctuations of the membranes and fluctuations in the positions of the stickers along the membranes as in Ref. [10]. The underlying theoretical framework is rather general and can incorporate any type of interaction between the various membrane components and the second surface. However, in order to eliminate some parameters from the problem, we will focus here on the situation in which the interaction of the ‘‘bare’’ or ‘‘naked’’ lipid bilayer with the second surface is effectively repulsive and of shorter range than the sticker-mediated attraction. Thus, we will focus on membranes that do not adhere to the second surface in the absence of stickers.

We show that sticker-mediated adhesion frequently leads to phase separation within the membrane as found in several recent studies [13,15,16]. However, one important message of our article is that there are *three distinct* mechanisms for this process of adhesion-induced phase separation.

First, we study membranes with flexible stickers that experience attractive cis interactions within the same membrane, see Sec. II. In this case, which was announced but not described in a previous Rapid Communication [13], the unbound membrane undergoes phase separation provided the attractive strength W of the cis interactions exceed a certain threshold value W_c . We find that this threshold value is significantly reduced if the membrane adheres to another surface. This reduction represents a renormalization of the cis interactions by the confined membrane fluctuations.

Second, we study rigid stickers that experience only repulsive (hard-core) cis interactions within the same membrane, see Sec. III. Now, the unbound membrane will always have a homogeneous or uniform composition. However, when bound to the substrate surface, such a membrane can also undergo phase separation. This process is driven by an effective line tension that arises from the shape fluctuations of the membrane and, thus, is of purely entropic origin. A similar mechanism has recently been described for stickers with an increased lateral size [13]. The underlying fluctuation mechanism can be suppressed by a sufficiently large lateral tension as discussed in Sec. IV.

Third, we study membranes with more than two components that contain both stickers and repellers, see Sec. V. The latter types of molecules are nonadhesive but protrude from the membrane surface and, thus, impose a steric barrier for the adhesion. We will focus on the case where the cis interactions between the stickers and repellers are purely repulsive. In this case, one may integrate over the composition variables and derive an effective potential for the membrane-membrane interactions. As a result, we find that this effective potential has a potential barrier and, thus, may lead to continuous or discontinuous unbinding transitions depending on

the height of this barrier [14]. Similar mechanisms for adhesion-induced phase separation resulting from an effective potential barrier have been recently discussed in Refs. [15] and [16].

In this way, we extend previous work on adhesion-induced phase separation as discussed in Refs. [13,15,16] and provide a *unified* conceptual framework for the different possible mechanisms that lead to this process. In order to exhibit the generic behavior related to these different mechanisms, we study an extended range for the parameters of our models. However, as discussed at the end of our paper, the parameter range studied here includes those parameter values that are applicable to real systems and, thus, accessible to experiments.

II. STICKERS WITH ATTRACTIVE CIS INTERACTIONS

A systematic theory for a multicomponent membrane with anchored stickers in contact with a substrate has to include a field l for the local separation between the membrane and the substrate and a concentration field n of the stickers. It is convenient to discretize the substrate into a two-dimensional square lattice with lattice constant a . Sticker positions can then be described by occupation numbers $n_i = 0$ or 1 where $n_i = 1$ indicates the presence of a sticker at lattice site i .

In general, the effective Hamiltonian (or configurational energy) of the decorated membrane will contain several terms [10] corresponding to the bending energy of the membrane, to the membrane/surface interactions, and to the interactions between the stickers. Each of these terms may depend on several parameters. In the present section, we will consider the simplest bending energy in which all membrane patches have the same bending rigidity irrespective of the absence or presence of stickers. In this way, we will focus on the effects of attractive cis interactions between the stickers.

Thus, let us consider a grand canonical Hamiltonian that has the general form [10]

$$\mathcal{H}\{l, n\} = \mathcal{H}_{el}\{l\} + \sum_i n_i [V(l_i) - \mu] + \sum_{\langle ij \rangle} W_{ij} n_i n_j, \quad (1)$$

where the elastic term

$$\mathcal{H}_{el}\{l\} = \sum_i \frac{\kappa}{2a^2} (\Delta_d l_i)^2 \quad (2)$$

represents the bending energy of the membrane with bending rigidity κ . The discretized Laplacian Δ_d is given by

$$\Delta_d l_i = \Delta_d l_{x,y} = l_{x+a,y} + l_{x-a,y} + l_{x,y+a} + l_{x,y-a} - 4l_{x,y}. \quad (3)$$

The potential $V(l_i)$ describes the transinteraction of an individual sticker with the substrate, and the relative chemical potential of the stickers with respect to the nonadhesive component is denoted by μ . We consider the short-ranged sticker potential

$$V(l_i) = U\theta(l_v - l_i) = U \quad \text{for } l_i \leq l_v = 0 \quad \text{for } l_i > l_v, \quad (4)$$

which depends on the sticker binding energy $U < 0$ and the potential range l_v . The step function $\theta(x)$ is equal to 0 for $x < 0$, and equal to 1 for $x \geq 0$. The cis interactions of the stickers are taken to be

$$\begin{aligned} W_{ij} &= W \quad \text{for nearest neighbors } i, j, \\ &= 0 \quad \text{otherwise,} \end{aligned} \quad (5)$$

with interaction strength $W \leq 0$. After a rescaling of the separation field according to

$$z \equiv (l/a)\sqrt{\kappa/T}, \quad (6)$$

the number of independent parameters turns out to be four: The reduced sticker binding energy $|U|/T$, the rescaled potential range $z_v = (l_v/a)\sqrt{\kappa/T}$, the reduced interaction strength W/T , and the reduced chemical potential μ/T . Here, T denotes the temperature in energy units [17]. Instead of the chemical potential, we will, in the following, use its conjugate variable, namely the sticker concentration $X = \langle n_i \rangle / a^2$, to describe the phase behavior.

A. Mean-field theory for concentration field

To develop a mean-field theory for the concentration field n of the stickers, we use the variational principle

$$\mathcal{F} \leq \mathcal{F}_o + \frac{1}{A} \langle \mathcal{H} - \mathcal{H}_o \rangle_o \quad (7)$$

with

$$\mathcal{H}_o\{l, n\} \equiv \mathcal{H}_{el}\{l\} + \sum_i n_i [V(l_i) - \mu + B], \quad (8)$$

where B is a variational parameter and A the membrane area. The brackets $\langle \cdot \rangle_o$ denote averages with respect to \mathcal{H}_o , and \mathcal{F}_o is the free energy related to \mathcal{H}_o . The effective Hamiltonian \mathcal{H}_o is linear in n and corresponds to $W=0$ and the shifted chemical potential $\mu - B$. A detailed derivation of the free energy for $W=0$ based (i) on an exact summation of the sticker degrees of freedom n_i and (ii) on a new method to determine the adhesion free energy of a homogeneous membrane by Monte Carlo simulations is described in Appendix A. The resulting expression for the free energy is given by Eq. (A10). The free energy \mathcal{F}_o is then obtained by replacing μ in Eq. (A10) by $\mu - B$. Evaluation of $\langle \mathcal{H} - \mathcal{H}_o \rangle_o$ now leads to

$$\mathcal{F} \leq \mathcal{F}_o - \frac{B}{A} \sum_i \langle n_i \rangle_o + \frac{1}{A} \sum_{\langle ij \rangle} W_{ij} \langle n_i n_j \rangle_o \quad (9)$$

$$\leq \mathcal{F}_o - \frac{B}{a^2} \langle n_i \rangle_o + \frac{2W}{a^2} \langle n_i \rangle_o^2 \equiv \mathcal{F}_>. \quad (10)$$

The second inequality holds for a square lattice with four nearest neighbors and interactions as in Eq. (5) since the correlation function $\langle n_i n_j \rangle_o - \langle n_i \rangle_o^2$ is nonnegative due to fluctuation-induced attractive interactions between bound stickers, which has been checked explicitly in our Monte Carlo (MC) simulations, see also Fig. 6. Now minimizing $\mathcal{F}_>$ with respect to the variational parameter B leads to the self-consistency equation

$$B = 4W \langle n_i \rangle_o, \quad (11)$$

where $\partial \mathcal{F}_o / \partial B = -\partial \mathcal{F}_o / \partial \mu = \langle n_i \rangle_o / a^2$ has been used.

B. Phase behavior from mean-field theory and Monte Carlo (MC) simulations

The phase behavior in the mean-field theory for the concentration field n can be derived numerically from Eqs. (10) and (11). In Fig. 1, we display phase diagrams for the rescaled potential range $z_v = 0.1$ and several values of the cis-interaction strength W as a function of the sticker concentration $X = \langle n_i \rangle / a^2$ and the sticker binding energy U . The diagram at $W/T = -0.3$ contains a bound and an unbound phase that are separated by a single line of continuous unbinding transitions. The membrane is bound for high concentrations or high binding energies of the stickers, and unbound for low concentrations or low binding energies. This transition belongs to the same universality class as the one for $W=0$ [10] and arises from the renormalization of the attractive membrane/surface interactions by thermally excited shape fluctuations [18], see Appendix A.

For larger absolute values $|W|$ of the cis-interaction strength, the diagrams contain two-phase regions where an unbound phase with a low concentration of stickers and a bound phase with a higher sticker concentration coexist. The coexistence regions end in tricritical points. For binding energies $|U|$ below the tricritical value $|U_{tc}|$, the unbinding transition of the membrane is continuous. For $|U| > |U_{tc}|$, the unbinding transition is discontinuous and is then coupled to phase separation within the membrane. At large absolute values $|U|$ of the sticker binding energy, the sticker concentrations of the two coexisting phases vary only slightly with U since the majority of the stickers is already bound.

The mean-field phase diagrams at the larger rescaled potential range $z_v = 0.5$ as displayed in Fig. 2 reveal a more complicated phase behavior with different topologies of the shaded coexistence regions. In particular, the diagrams at the cis-interactions strengths $W/T = -0.8$ and $W/T = -0.84$ contain regions where two bound phases coexist. Thus, for intermediate values of the cis interactions W/T and the transinteractions U/T , mean-field theory predicts that the system exhibits *four* different states as a function of the sticker concentration X : (i) at large sticker concentrations, the membrane composition is uniform and the membrane is bound; (ii) at intermediate values of X , the membrane undergoes phase separation that leads to two types of domains. Both types of domains are bound to the second surface. However, since the two types of domains differ in their sticker concentrations, their mean separation from the second

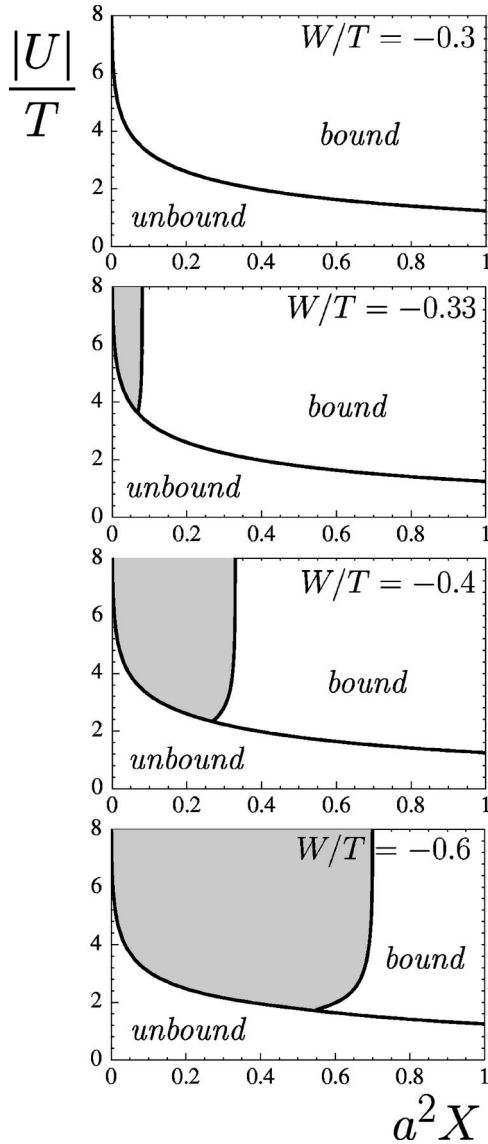


FIG. 1. Mean-field phase diagrams for a membrane with flexible stickers depending on the sticker concentration X and the binding energy U . The rescaled quantities $a^2 X$ and U/T are dimensionless where a is the lattice constant and T is the temperature in energy units. The dimensionless potential range of the stickers is $z_v = 0.1$. Above a critical value of the cis-interaction strength $|W|$, a separation into an unbound phase with a low concentration of stickers and a bound phase with a higher sticker concentration can be observed. The extent of the shaded two-phase coexistence region increases with $|W|$.

surface will be different. Thus, one has a bound state with a nonuniform surface separation. Such a state resembles the state of a thin liquid film at a prewetting transition [19]; (iii) as X is further decreased, the bound membrane becomes again uniform, and (iv) finally, at very low values of X , it unbinds in a continuous fashion, i.e., in the same way as for a one-component membrane.

In Figs. 3 and 4, we compare the phase diagrams from the mean-field theory and from Monte Carlo (MC) simulations with the full Hamiltonian (1). In the simulations, we determine the concentration $X = \langle n_i \rangle / a^2$ as a function of the

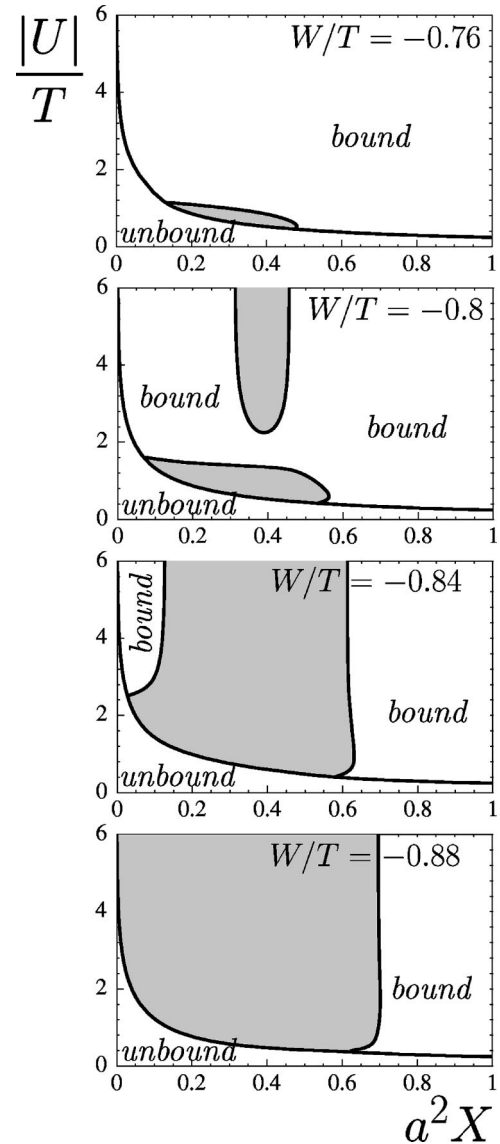


FIG. 2. Mean-field phase diagrams as a function of the dimensionless concentration $a^2 X$ and binding energy U/T , compare Fig. 1, for flexible stickers with the dimensionless potential range $z_v = 0.5$. The two-phase coexistence regions are shaded. Because of the dominance of the cis interactions at the larger potential range $z_v = 0.5$, the diagrams at the interaction strengths $W/T = -0.8$ and $W/T = -0.84$ include regions where two bound phases coexist, see text.

chemical potential μ of the stickers. A first-order transition is reflected in a discontinuity of the concentration X at a certain chemical potential μ_* . The two limiting values X_1 and X_2 at μ_* correspond to the concentrations of the coexisting phases. In order to determine these concentrations, we typically perform 10 to 20 MC simulations with up to 10^7 steps per lattice site at different chemical potentials μ above and below μ_* for fixed binding energy U and interaction strength W on lattices with up to 120×120 lattice sites.

It is important to note that lateral phase separation can already be observed at interaction strengths $|W|$ that are significantly below the critical interaction strength $|W_c|$ of the

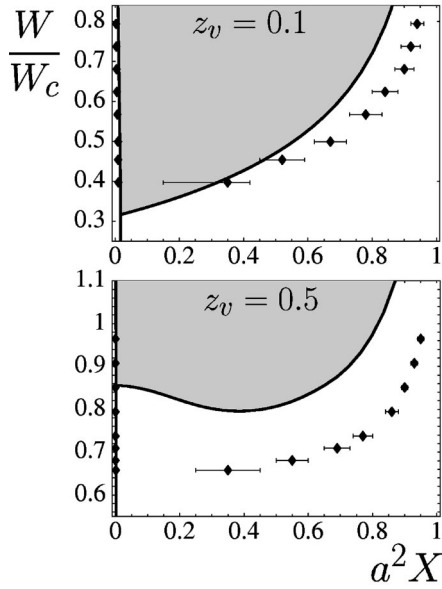


FIG. 3. Phase diagrams depending on the dimensionless concentration $a^2 X$ and cis-interaction strength W of flexible stickers with binding energy $U/T = -5$ and the rescaled potential ranges $z_v = 0.1$ and 0.5 . Lines and shaded coexistence regions correspond to the mean-field theory, data points to MC simulations. The interaction strength W is rescaled by the critical value W_c of the two-dimensional lattice gas with $W_c/T = -1$ for the mean-field calculations and $W_c/T = -2 \ln(1 + \sqrt{2})$ for the MC data.

two-dimensional lattice gas with Hamiltonian

$$\mathcal{H}_{lg}\{n\} = \sum_{\langle ij \rangle} W_{ij} n_i n_j - \mu \sum_i n_i, \quad (12)$$

and nearest-neighbor cis interaction as in Eq. (5). The critical interaction strength of the two-dimensional lattice gas is $W_c/T = -2 \ln(1 + \sqrt{2})$, and $W_c/T = -1$ in the mean-field theory. For the rescaled potential range $z_v = 0.1$ and the bind-

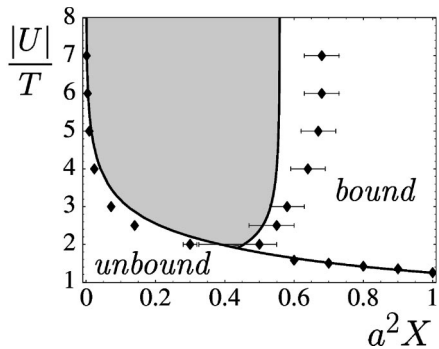


FIG. 4. Phase diagram for a membrane with flexible stickers depending on the dimensionless sticker concentration $a^2 X$ and binding energy U/T . The dimensionless potential range of the stickers is $z_v = 0.1$, and the cis-interaction strength is $W = 1/2W_c$. The lines and shaded coexistence region are obtained from the mean-field theory, the data points from MC simulations with the full Hamiltonian (1). The critical interaction strength of the two-dimensional lattice gas is $W_c/T = -1$ in the mean-field theory and $W_c/T = -2 \ln(1 + \sqrt{2})$ for the MC simulations.

ing energy $U/T = -5$, the tricritical point where the phase separation sets in can be estimated from the MC data of Fig. 3(a) as $W_{tc}/W_c = 0.35 \pm 0.05$ and agrees within the statistical errors with the tricritical point of the mean-field phase diagram. Thus, for $z_v = 0.1$, phase separation already occurs at interaction strengths that are about one third of the critical interaction strength W_c of the two-dimensional lattice gas. The lateral phase behavior therefore is dominated by entropic forces between the stickers that are induced by shape fluctuations of the membrane. Since these shape fluctuations of the bound membrane are strongest at the unbinding point, the lateral phase separation is coupled with the unbinding transition of the membrane.

For the larger rescaled potential range $z_v = 0.5$, the tricritical point as obtained from the Monte Carlo data of Fig. 3(b) is located at $W_{tc}/W_c = 0.65 \pm 0.05$. The phase separation thus is predominantly caused by the enthalpic cis interactions. As a consequence of the dominance of the cis interactions at larger rescaled potential ranges z_v , the mean-field phase diagrams for $W/T = -0.8$ or -0.84 and $z_v = 0.5$ include regions where two bound phases coexist as shown in Fig. 2, since the critical concentration of the two-dimensional lattice gas with Hamiltonian (12) is $X_c = 0.5/a^2$.

A comparison of the mean field and the MC phase diagram for the rescaled potential range $z_v = 0.1$ and the cis-interaction strength $W = 1/2W_c$ is presented in Fig. 4. As in Fig. 3(a), we find relatively good agreement of the two phase diagrams. At the larger rescaled potential range $z_v = 0.5$ where the phase separation only occurs at larger absolute values $|W|$ of the cis-interaction strength, the difference of the mean field and MC phase diagrams is more pronounced, see Fig. 3(b).

The lateral phase separation is illustrated in Fig. 5 where we see configurations from canonical Monte Carlo simulations with fixed sticker concentrations $X = 0.45/a^2$, $0.3/a^2$, and $0.1/a^2$ for the rescaled potential range $z_v = 0.1$ and the interaction strength $W = 1/2W_c$. We see a separation into a bound phase with a high concentration of bound stickers shown in black and an unbound white phase almost free of stickers with a much larger membrane separation. With decreasing sticker concentration, the extent of the bound phase shrinks. For a comparison, Monte Carlo configurations for $W = 0$ are shown in Fig. 6. Due to fluctuation-induced interactions, black bound stickers have some tendency to cluster but the membrane does *not* phase separate in agreement with Ref. [10].

III. STICKERS WITH ENLARGED BENDING RIGIDITY

For stickers that differ in their bending rigidity from the lipid matrix, the grand canonical Hamiltonian can be written as

$$H\{l, n\} = \sum_i \frac{\kappa}{2a^2} (\Delta_d l_i)^2 + \sum_i n_i \left(\frac{\kappa_s - \kappa}{2a^2} (\Delta_d l_i)^2 + V(l_i) - \mu \right) \quad (13)$$

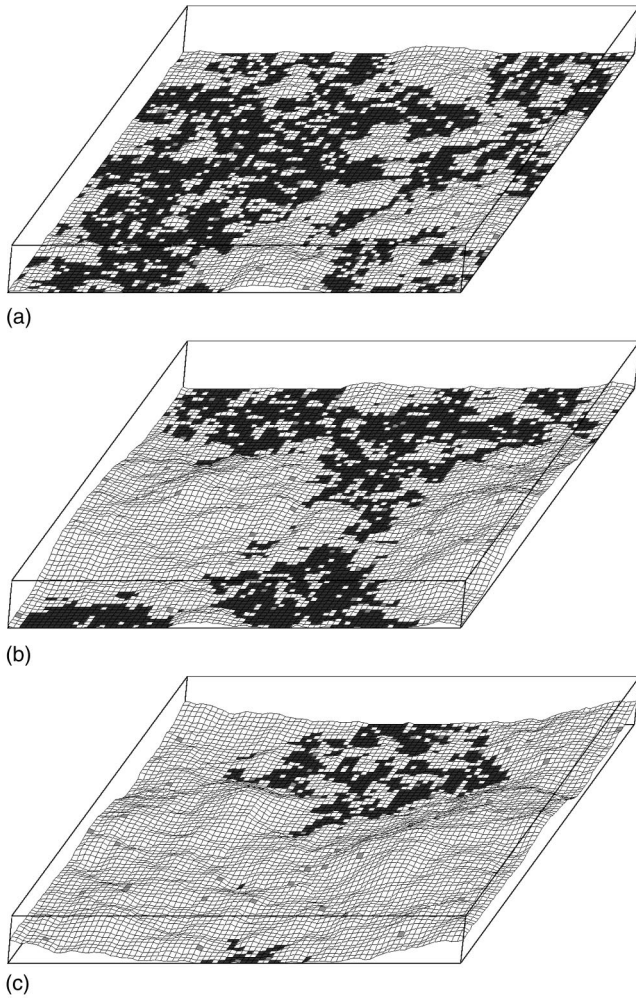


FIG. 5. Typical MC configurations of a two-component membrane with flexible stickers of cis-interaction strength $W = W_c/2 = -T \ln(1 + \sqrt{2})$, binding energy U , and potential range $z_v = 0.1$. Bound stickers are black, unbound stickers grey, and nonadhesive segments are white. The fixed sticker concentration is $X = 0.45/a^2$, $0.3/a^2$, and $0.1/a^2$ (bottom to top). The membrane phase separates into a bound phase with a high concentration of stickers, and an unbound phase with a low sticker concentration.

in the absence of cis-interactions. Here, κ_s denotes the bending rigidity of the stickers, and κ is the rigidity of the lipid bilayer. The adhesion potential $V(l_i)$ is again given by Eq. (4) with binding energy U and potential range l_v . The discretized Laplacian Δ_d is defined in Eq. (3). As before, a denotes the lattice constant, and μ the relative chemical potential of the stickers.

Now, the phase behavior can be characterized by the reduced binding energy U/T , the rescaled potential range $z_v = (l_v/a)\sqrt{\kappa/T}$, the sticker concentration $X = \langle n_i \rangle / a^2$, and the reduced sticker rigidity κ_s/κ . Because of the elastic contribution of the stickers, a summation of the sticker degrees of freedom in the partition function does not lead to a simplification of the problem, as in the case of flexible stickers without cis interactions, see Appendix A. We therefore determine the phase behavior by Monte Carlo simulations with the full Hamiltonian (13) as described in the previous section.

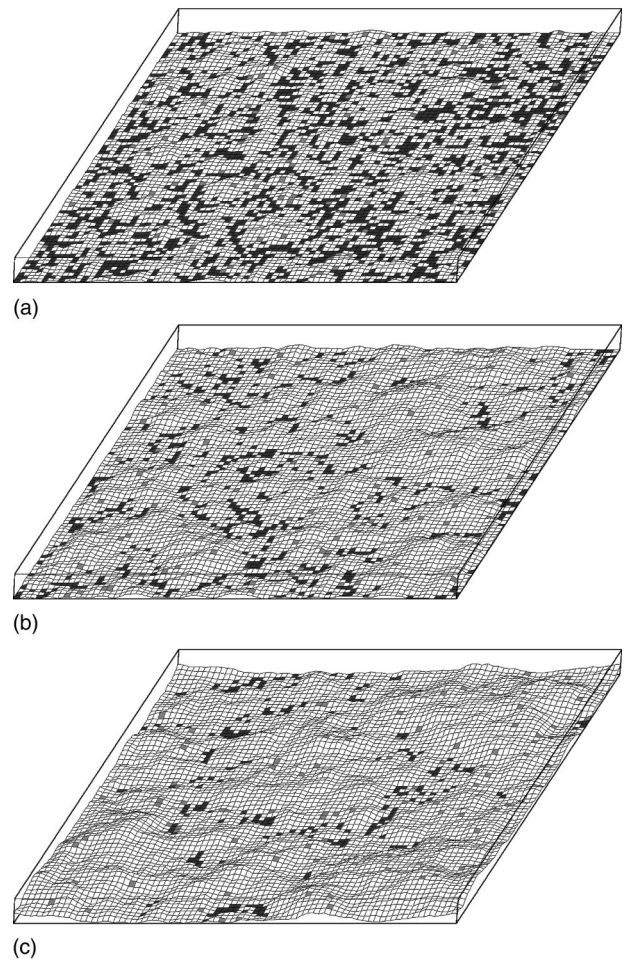


FIG. 6. Typical MC configurations of a two-component membrane with flexible stickers in the absence of cis interactions. Bound stickers are black, unbound stickers gray, and nonadhesive segments are white. The average separation of the membrane increases continuously as the sticker concentration is reduced. Bound stickers have some tendency to cluster but the membrane does *not* phase separate.

In Fig. 7, we see the phase behavior as a function of the concentration X and the reduced sticker rigidity κ_s/κ for $U/T = -5$, and thus for a relatively high sticker binding energy. Both diagrams exhibit again two-phase regions where an unbound phase with a very small sticker concentration X_1 and a bound phase with a higher concentration X_2 coexist. Since cis interactions are absent in the Hamiltonian (13), the phase separation is now only induced by the shape fluctuations of the membrane. The two-phase regions end in tricritical points given by $\kappa_s/\kappa = 1.3 \pm 0.3$ for $z_v = 0.1$ and by $\kappa_s/\kappa = 1.5 \pm 0.5$ for $z_v = 0.5$. Below the tricritical points, the unbinding transition is continuous in accordance with Appendix A where we present a general argument that shows that multicomponent membranes with flexible stickers, i.e., with stickers of bending rigidity $\kappa_s = \kappa$, do not phase separate in the absence of attractive cis interactions between the stickers.

At high sticker rigidities, the coexistence concentrations reach the values $X_1 = 0$ and $X_2 = (0.85 \pm 0.02)/a^2$ for z_v

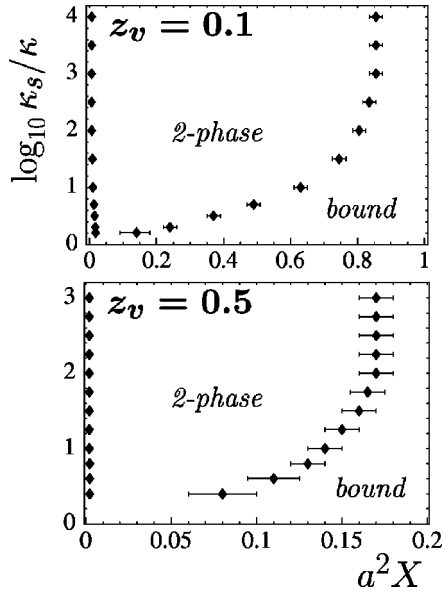


FIG. 7. Phase diagrams depending on the bending rigidity κ_s and the dimensionless concentration $a^2 X$ of the stickers that have the binding energy $U = -5T$ and the dimensionless potential ranges $z_v = 0.1$ (top) and 0.5 (bottom). The sticker bending rigidity κ_s is rescaled by the bending rigidity κ of the lipid matrix. Here, the only cis interactions between the stickers arise from the mutual exclusion at the same membrane patch.

$= 0.1$ and $\kappa_s/\kappa \geq 1000$, and $X_2 = (0.17 \pm 0.01)/a^2$ for $z_v = 0.5$ and $\kappa_s/\kappa \geq 100$, see Fig. 7. The dependence of the phase behavior on the rescaled potential range z_v is explicitly shown in Fig. 8. The width of the coexistence region decreases with increasing z_v as fluctuation effects become weaker: With increasing potential range, bound stickers become less restrictive to the membrane fluctuations.

In order to understand the strong tendency of rigid stickers to phase separate, let us consider a cluster of densely packed bound stickers with $n_i = 1$ and $l_i \leq l_v$ that is surrounded by a nonadhesive membrane segment with $n_i = 0$. In the limit of large sticker rigidities κ_s , the membrane distance l_i at the lattice sites directly adjacent to the sticker cluster has to be smaller or close to the potential range l_v to avoid high

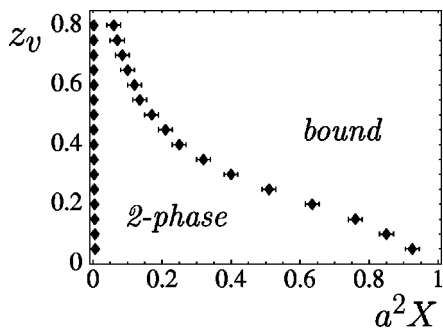


FIG. 8. Phase diagram depending on the dimensionless sticker concentration $a^2 X$ and the dimensionless potential range z_v for stickers with bending rigidity $\kappa_s = 1000\kappa$ and binding energy $U = -5T$. As in Fig. 7, the only cis interactions between the stickers arise from the mutual exclusion at the same membrane patch.

curvatures at the cluster boundary, see Eq. (3). Thus, the binding of the sticker cluster leads to an additional stripe of “bound” or “nearly bound” (but nonadhesive) lattice sites around the sticker array that costs entropy by restricting the membrane fluctuations. Since the membrane separation around clusters of flexible stickers with $\kappa_s = \kappa$ is clearly less restricted, large sticker rigidities induce an additional effective line tension at the boundary of bound sticker clusters that favors the aggregation of the clusters, and thus, favors lateral phase separation. A similar process of phase separation due to an effective line tension arising from the interplay of shape fluctuations and sticker clusters has recently been found for stickers with increased lateral size [13].

Attractive fluctuation-induced forces have also been shown to exist between non-adhesive membrane inclusions with higher bending rigidity [20,21]. These forces are considerably weaker than the entropic interactions between rigid stickers and contribute to the lateral phase separation of the membrane only at relatively large inclusion rigidities in a significant way [22].

IV. EFFECT OF LATERAL MEMBRANE TENSION

Biological and biomimetic membranes are often under lateral tension. This tension acts to suppress membrane fluctuations and will therefore also affect the fluctuation-induced phase separation that was studied in the previous sections. A lateral tension σ leads to the additional term

$$\mathcal{H}_\sigma\{l\} = \sum_i \frac{\sigma}{2} (\nabla_d l_i)^2 \quad (14)$$

in the Hamiltonian where

$$(\nabla_d l_i)^2 = (\nabla_d l_{x,y})^2 = (l_{x+a,y} - l_{x,y})^2 + (l_{x,y+a} - l_{x,y})^2 \quad (15)$$

describes the local area increase of the curved membrane with respect to the planar substrate. As before, neighboring sites at the membrane edges are defined via periodic boundary conditions. After the rescaling (6) of the distance field l , the additional dimensionless parameter corresponding to σ turns out to be the reduced tension $\sigma a^2/\kappa$.

The phase separation of membranes with rigid stickers is only induced by fluctuation-induced interactions. In the presence of a lateral tension, the grand canonical Hamiltonian for these membranes is given by the sum of Eqs. (13) and (14). In Fig. 9, we display Monte Carlo phase diagrams for stickers with bending rigidity $\kappa_s = 1000\kappa$ as a function of the sticker concentration $X = \langle n_i \rangle / a^2$ and the reduced tension $\sigma a^2/\kappa$. At small lateral tensions σ , the concentrations of the coexisting phases agree with the tensionless case, see Fig. 8. At higher tensions, the width of the coexistence region decreases due to the suppression of the fluctuation-induced interactions between bound stickers.

It is important to note that the tensions at which a decrease of the concentration X_2 of the bound phase can be observed are relatively high. Lipid membranes typically rupture at tensions σ_r of a few millinewton per meter [23]. Taking $\sigma_r = 4mN/m$, a lattice constant $a = 5$ nm which is

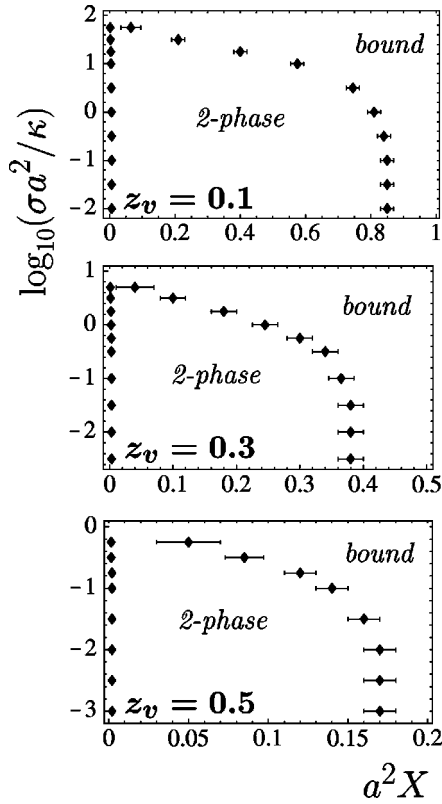


FIG. 9. Phase diagrams depending on the dimensionless sticker concentration $a^2 X$ and the dimensionless tension $\sigma a^2 / \kappa$ for stickers with bending rigidity $\kappa_s = 1000\kappa$ and binding energy $U = -5T$. The dimensionless potential ranges are $z_v = 0.1, 0.3,$ and 0.5 .

about the lipid bilayer thickness, and the bending rigidity $\kappa = 10^{-19}J$ leads to the estimate $\sigma_r a^2 / \kappa = 1$ or $\log_{10}(\sigma_r a^2 / \kappa) = 0$ for the maximum value of the reduced tension. The phase diagrams of Fig. 9 show that the tensions, which cause a significant decrease of the coexistence region, are already close to or even above this estimate for the maximum value.

In order to understand this behavior, one has to realize that membrane fluctuations are suppressed only on length scales that exceed the crossover length $\sqrt{\kappa/\sigma}$. On smaller scales, thermal fluctuations are still governed by the bending energy. The decrease of the coexistence regions in the phase diagrams of Fig. 9 sets in at values of the reduced tension $\sigma a^2 / \kappa$ that correspond to crossover lengths of only a few lattice constants. Thus, the relevant fluctuations turn out to be undulations of the nonadhesive membrane segments between the small clusters of bound stickers, see Fig. 6. A decrease of fluctuation interactions between the bound stickers then occurs if the crossover length $\sqrt{\kappa/\sigma}$ is comparable to or smaller than the mean distance between the sticker clusters. This interpretation agrees with the observation that the influence of an increasing lateral tension is most pronounced for the rescaled potential range $z_v = 0.5$. For this value of z_v , the concentration X_2 of the bound phase at low tensions has the smallest value and the corresponding distance between the sticker clusters has the largest value for the three cases displayed in Fig. 9.

V. MEMBRANES WITH STICKERS AND REPELLERS

Biological membranes often contain repulsive molecules that form a protective barrier, the glycocalyx. A systematic description should then include a concentration field that adopts three values, e.g., $n_i = 0, 1,$ and 2 for the neutral component, the stickers, and the repellers, respectively. In the absence of cis interactions, the grand-canonical Hamiltonian for a three-component membrane in contact with a substrate or wall can be written as

$$\mathcal{H}\{l, n\} = \mathcal{H}_{el}\{l\} + \sum_i \vartheta(n_i) [V_{n_i}(l_i) - \mu_{n_i}], \quad (16)$$

with $\vartheta(n_i) = 0$ for $n_i = 0$, and $\vartheta(n_i) = 1$ for $n_i = 1$ or 2 , where $V_1(l_i)$ denotes the attractive sticker potential and $V_2(l_i)$ the transinteraction of the repellers, and μ_1 and μ_2 are the relative chemical potentials corresponding to stickers and repellers, respectively. The elastic energy \mathcal{H}_{el} is again given by Eq. (2) assuming a uniform bending rigidity κ of the membrane. Summing out the degrees of freedom of the concentration field n as described in Appendix A now leads to the partition function

$$\mathcal{Z} = (1 + e^{\mu_1/T} + e^{\mu_2/T})^N \times \left[\prod_i \int_0^\infty dl_i \right] e^{-[\mathcal{H}_{el}\{l\} + \sum_i V_{ef}(l_i)]/T}, \quad (17)$$

with the total number of lattice sites N and the effective potential

$$V_{ef}(l_i) = -T \ln \frac{1 + e^{l\mu_1 - V_1(l_i)/T} + e^{l\mu_2 - V_2(l_i)/T}}{1 + e^{\mu_1/T} + e^{\mu_2/T}}. \quad (18)$$

In the following, we characterize the potentials V_1 and V_2 as square-well and square-barrier potentials of the form (4) with potential energies $U_1 < 0$ and $U_2 > 0$ and with potential ranges l_1 and l_2 . If the repellers have a larger potential range than the stickers, i.e., for $l_2 > l_1$, the effective potential reads

$$\begin{aligned} V_{ef}(l_i) &= U_{co} \quad \text{for } 0 < l_i < l_1 \\ &= U_{ba} \quad \text{for } l_1 < l_i < l_2 \\ &= 0 \quad \text{for } l_2 < l_i, \end{aligned} \quad (19)$$

with

$$U_{co} \equiv -T \ln \frac{1 + e^{(\mu_1 - U_1)/T} + e^{(\mu_2 - U_2)/T}}{1 + e^{\mu_1/T} + e^{\mu_2/T}}, \quad (20)$$

and

$$U_{ba} \equiv -T \ln \frac{1 + e^{\mu_1/T} + e^{(\mu_2 - U_2)/T}}{1 + e^{\mu_1/T} + e^{\mu_2/T}}, \quad (21)$$

as displayed in Fig. 10. Because of $U_2 > 0$ we also have $U_{ba} > 0$, and from $U_1 < 0$ we conclude that $U_{co} < U_{ba}$. The effective potential thus contains a potential barrier with

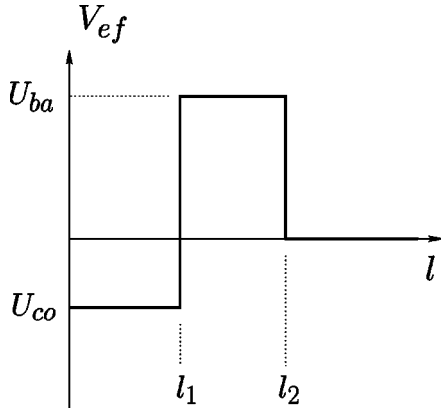


FIG. 10. Schematic shape of the effective potential V_{ef} as a function of the surface separation l , see Eq. (19), for a membrane with flexible stickers and repellers in the absence of cis interactions.

height U_{ba} for $l_1 < l_i < l_2$. Bound states of the membrane are only possible if the energy U_{co} for membrane contacts with $l_i < l_1$ is negative, i.e., for

$$e^{\mu_1/T}(e^{-U_1/T} - 1) > e^{\mu_2/T}(1 - e^{-U_2/T}), \quad (22)$$

which reduces to the condition $\mu_1 - U_1 > \mu_2$ for large sticker and repeller energies with $|U_1|/T \gg 1$ and $U_2/T \gg 1$.

For membranes confined to a potential well with width l_1 , the excess free energy is given by $V_{fl}(l_1) \sim T^2/\kappa l_1^2$ [24]. The free energy difference between the bound and the unbound state of a membrane with adhesion potential (19) therefore can be written as $\Delta F = -|U_{co}| + cT^2/\kappa l_1^2$ where c is a dimensionless coefficient. An estimate for the contact energy U_{co}^* at which the membrane unbinds thus follows as

$$|U_{co}^*| = cT^2/\kappa l_1^2 \quad (23)$$

since the free energy difference ΔF has to be zero at the unbinding point.

The character of the unbinding transition now depends on the height of the potential barrier that induces a line tension between bound and unbound membrane segments. As shown in Ref. [14], the unbinding transition is discontinuous for relatively strong barriers with

$$U_{ba}(l_2 - l_1)^2 \gg |U_{co}^*| l_1^2, \quad (24)$$

and continuous for weak barriers with $U_{ba}(l_2 - l_1)^2 \ll |U_{co}^*| l_1^2$. A discontinuous transition implies the coexistence of a bound phase with a high concentration of stickers and an unbound phase with a low sticker concentration. Therefore, sufficiently strong barriers also lead to lateral phase separation and sticker aggregation. This should especially apply to membranes containing relatively rigid repellers that can be characterized by high values of U_2 and thus induce large potential barriers U_{ba} according to Eq. (19).

It is important to note that, in the present situation, the phase separation is *not* induced by membrane fluctuations as in the previous sections. On the contrary, since the transition value $|U_{co}^*|$ of the contact energy increases with the temperature T and decreases with the bending rigidity κ , membranes

with more pronounced shape fluctuations require larger potential barriers for a discontinuous unbinding transition and lateral phase separation as follows from Eq. (24). An increase of membrane fluctuations thus reduces the tendency of the membrane to phase separate. As stated above, the phase separation of a multicomponent membrane with the effective adhesion potential (19) is caused by the potential barrier that induces a line tension between bound and unbound membrane segments. The adhesion-induced phase separation reported in Ref. [16] where the membrane is in an external harmonic potential and the stickers couple linearly to the separation field is caused by a similar mechanism [25].

VI. CONCLUSION

In this article, we have identified and distinguished three different mechanisms for lateral phase separation during the adhesion of multicomponent membranes. In the first mechanism, the shape fluctuations of the membrane lead to a renormalization of the cis interactions between flexible stickers that are taken to have the same bending rigidity as the membrane matrix. Phase separation and discontinuous unbinding thus occurs at cis-interaction strengths $|W|$ which are significantly smaller than the critical interaction strength $|W_c|$ for the flat membrane. The renormalization of the cis interactions can also be understood as a nontrivial coupling with collective entropic interactions induced by the membrane fluctuations.

A second mechanism is effective for stickers that have a larger bending rigidity than the lipid matrix. The membrane fluctuations then induce an additional entropic line tension between bound and unbound membrane domains that leads to lateral phase separation also in the absence of any attractive cis interactions. A comparable increase of entropic interactions due to an effective line tension has been previously reported for stickers with increased lateral size [13].

The strength of these two fluctuation-induced mechanisms is reflected in the extent of the coexistence regions. For large binding energies $|U|$ and rigidities κ_s of the stickers, this strength is determined by a single parameter, the rescaled potential range $z_v = (l_v/a)\sqrt{\kappa/T}$, which is a function of the sticker potential range l_v in units of the lattice constant a , the bending rigidity κ of the lipid matrix, and the temperature T . The extent of the coexistence regions decreases with increasing rescaled potential range z_v because the shape fluctuations (i) are less restricted by bound stickers with larger potential ranges l_v and (ii) get weaker with increasing bending rigidity κ or decreasing temperature T . For lipid membranes, the dimensionless factor $\sqrt{\kappa/T}$ is around 3 or 4 [26], and the lattice constant a should be taken as the cutoff length for the membrane fluctuations. As mentioned in the introduction, this cutoff length is around 6 nm for lipid bilayers with a thickness of 4 nm [11]. Since the sticker potential range l_v may vary from a few angstroms for sticky lipids to several nanometers for adhesion proteins, the rescaled potential ranges considered in this article are accessible to experiments on real adhesion molecules.

Studying the influence of lateral membrane tensions on the phase behavior leads to a deeper understanding of the

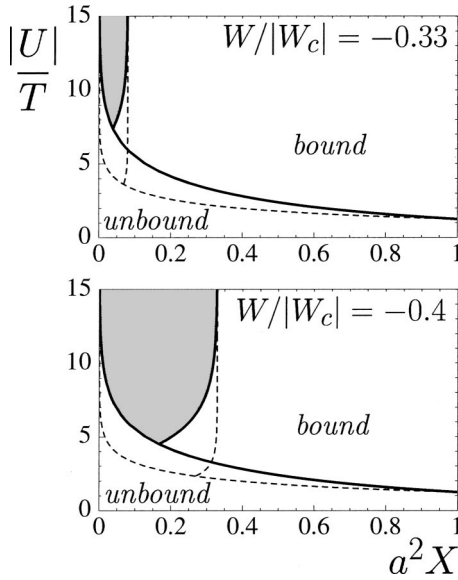


FIG. 11. Mean-field phase diagrams as a function of the dimensionless concentration a^2X and binding energy U/T : (Thick lines) A pair of two-component membranes with identical sticker concentration a^2X ; and (Dashed lines) A membrane with sticker concentration X in front of a homogeneous substrate. The dimensionless potential range is $z_v = 0.1$. The cis-interaction strength is denoted by W , and W_c is the critical interaction strength for a planar membrane.

fluctuation-induced interactions. Since the extent of the coexistence regions decreases only at relatively large lateral tensions, the relevant fluctuations for the entropic forces turn out to be fluctuations on the scale of the average separation of the stickers which is close to the lattice constant a if the sticker concentration is sufficiently large.

A third mechanism of lateral phase separation exists for membranes that contain both stickers and repellers. If the transinteraction of the repellers has a longer range than the sticker potential, the effective adhesion potential, which results from a summation of the degrees of freedom of the concentration field, contains a potential barrier. This barrier induces an effective line tension between bound and unbound membrane segments. For large enough potential barriers, the line tension leads to a discontinuous unbinding transition, and thus, to lateral phase separation. An increase of membrane fluctuations effectively reduces the barrier, and therefore also reduces the tendency of the membrane to phase separate in contrast to the first two mechanisms.

We have considered here the simplest adhesion geometry that consists of a single multicomponent membrane with stickers in contact with a homogeneous substrate. In Appendix B, we compare this simple geometry with the situation where two multicomponent membranes interact via “lock-and-key” stickers. We find that the phase behavior is rather similar in both geometries. In particular, the phase diagrams agree in the regime of high sticker binding energies, see Fig. 11, where almost all stickers are bound, provided the membranes have equal sticker concentrations and the transinteraction of the stickers can be described in both cases by the same molecular adhesion potential. The regime of high sticker binding energies applies to biologically relevant ad-

hesion molecules that are expected to have binding energies $|U|/T \gg 1$ [27].

From the experimental point of view, lateral phase separation has been observed in some biomimetic systems such as (i) membranes containing cationic lipids in contact with a negatively charged surface [28], (ii) membranes with biotinylated lipids that are bound to another biotinylated surface via streptavidin [29], and (iii) membranes with homophilic csa receptors from the slime mould *Dictyostelium discoideum* [30]. One system that does not seem to exhibit adhesion-induced phase separation are (iv) neurons, which adhere to laminin or fibronectin covered silica surfaces [31].

The first experimental system (i) corresponds to stickers that experience repulsive and attractive electrostatic cis and trans interactions. Such interactions lead to an effective increase of the sticker size. As shown in Ref. [13], the adhering membrane undergoes phase separation if the sticker size is larger than the size of the nonadhesive membrane patches and the potential range of the trans interactions is sufficiently small. The experimental systems (ii) and (iii), on the other hand, contained both stickers and repeller molecules that were supposed to mimic the glycocalyx of cell membranes. Therefore, the observed phase separation is presumably induced by a potential barrier in the effective membrane-surface interaction, as shown schematically in Fig. 10. Finally, all our phase diagrams exhibit bound states with a uniform surface separation as observed experimentally for neurons on silica surfaces.

The theoretical work described here focused on the structure of the membrane/sticker systems in equilibrium. It is also of interest to study the dynamics of these systems, which involves both a coarsening of the intramembrane domains and the relaxation of the membrane/surface separation. In general, one may then have to include hydrodynamic effects, see, e.g., Ref. [32]. Likewise, one may study related processes away from equilibrium such as (i) the unbinding of the sticker bonds under a time-dependent load force [33,34] or (ii) the interactions between the membrane and cytoskeletal filaments, which involve active processes and are believed to be essential for cell adhesion, see, e.g., Ref. [12].

ACKNOWLEDGMENTS

We would like to thank R. R. Netz for helpful discussions, and S. Komura and D. Andelman for stimulating interactions.

APPENDIX A: FREE ENERGIES OF ADHESION

A. Homogeneous membranes

In this section, we present a method to determine the free energy of a homogeneous membrane that adheres to a substrate or “wall.” The conformations of the membrane can be described by the local separation l from the wall. After discretizing the substrate into a two-dimensional square lattice, the effective Hamiltonian, which is the sum of the bending energy [35] and the potential energy of the membrane, can be written as

$$\mathcal{H}\{l\} = \sum_i \left[\frac{\kappa}{2a^2} (\Delta_d l_i)^2 + V(l_i) \right], \quad (\text{A1})$$

where $l_i \geq 0$ is the separation at lattice site i , the parameter κ is the bending rigidity, and a the lattice constant. The interaction potential between the membrane and the wall is denoted by $V(l_i)$, and the discretized Laplacian Δ_d is given in Eq. (3). The same description holds for the interaction of two homogeneous membranes with bending rigidities κ_1 and κ_2 . Then, κ represents the effective bending rigidity $\kappa_1 \kappa_2 / (\kappa_1 + \kappa_2)$ [36]. In the following, we consider the square-well potential

$$V(l_i) = Tu \theta(l_v - l_i) = Tu \quad \text{for } l_i \leq l_v = 0 \quad \text{for } l_i > l_v, \quad (\text{A2})$$

which is characterized by the potential depth $Tu < 0$ and the potential range l_v . By introducing the rescaled separation field $z \equiv (l/a) \sqrt{\kappa/T}$, the parameters can be reduced to the dimensionless potential depth u and the rescaled potential range $z_v = (l_v/a) \sqrt{\kappa/T}$.

Thermally excited shape fluctuations of the membrane lead to an entropic repulsion between the membrane and the wall [24], and thus, to an unbinding transition at a critical value u_* of the potential depth that depends on the rescaled potential range z_v . For short-range potentials as Eq. (A2), the unbinding transition is continuous [10], i.e., the average separation continuously diverges according to $\langle l_i \rangle \sim (u - u_*)^{-1}$ close to the critical potential depth u_* . In order to determine the free energy, we consider here the contact probability

$$P_b \equiv \langle \theta(z_v - z_i) \rangle, \quad (\text{A3})$$

which is the expectation value for the fraction of bound membrane segments, i.e., membrane segments with $z_i < z_v$. The contact probability can be directly determined in Monte Carlo (MC) simulations as reported in Ref. [13]. The free energy per area A as given by

$$\mathcal{F} = -\frac{T}{A} \ln \left[\prod_i \int_0^\infty dl_i \right] e^{-\mathcal{H}\{l\}/T}, \quad (\text{A4})$$

is related to the contact probability P_b via

$$P_b = \frac{a^2}{T} \frac{\partial \mathcal{F}}{\partial u}. \quad (\text{A5})$$

Thus, the free energy for given rescaled potential range z_v is obtained from Monte Carlo data for the contact probability by the integration

$$\mathcal{F} = \mathcal{F}_{ub} - \frac{T}{a^2} \int_u^{u_*} du' P_b(u'), \quad (\text{A6})$$

where \mathcal{F}_{ub} denotes the free energy of the unbound membrane associated with the shape fluctuations.

B. Two-component membranes with flexible stickers:

Absence of cis interactions

In the absence of cis interactions, the grand canonical Hamiltonian (1) for membranes with flexible stickers is linear in the concentration field n . Summing out the sticker degrees of freedom in the partition function

$$\mathcal{Z} = \left[\prod_i \int_0^\infty dl_i \right] \left[\prod_i \sum_{n_i=0,1} \right] e^{-\mathcal{H}\{l,n\}/T}, \quad (\text{A7})$$

then leads to

$$\begin{aligned} \mathcal{Z} &= \left[\prod_i \int_0^\infty dl_i \right] e^{-\mathcal{H}_e\{l\}/T} \prod_i (1 + e^{[\mu - V(l_i)]/T}) \\ &= (1 + e^{\mu/T})^N \left[\prod_i \int_0^\infty dl_i \right] e^{-[\mathcal{H}_e\{l\} + \sum_i V_{ef}(l_i)]/T}, \end{aligned} \quad (\text{A8})$$

with the number of lattice sites N and the effective potential

$$V_{ef}(l_i) = -T \ln \frac{1 + e^{[\mu - U]/T}}{1 + e^{\mu/T}} \theta(l_v - l_i) \equiv U_{ef} \theta(l_v - l_i). \quad (\text{A9})$$

The effective potential is again a square-well potential with potential range l_v and the effective potential depth U_{ef} that depends on the chemical potential μ and the binding energy U of the stickers. The free energy per unit area $\mathcal{F} = -(T/A) \ln \mathcal{Z}$ therefore is obtained as in the previous section and reads

$$\mathcal{F} = -\frac{T}{a^2} \ln[1 + e^{\mu/T}] + \mathcal{F}_{ub} - \frac{T}{a^2} \int_u^{u_*} du' P_b(u'), \quad (\text{A10})$$

where the reduced potential depth u now is given by U_{ef}/T .

The sticker concentration $X \equiv -(\partial \mathcal{F} / \partial \mu) = \langle n_i \rangle / a^2$ then follows as

$$X = \frac{1}{a^2} \left[(1 - P_b) \frac{e^{\mu/T}}{1 + e^{\mu/T}} + P_b \frac{e^{[\mu - U]/T}}{1 + e^{[\mu - U]/T}} \right]. \quad (\text{A11})$$

At the continuous unbinding point, the contact probability P_b vanishes and the critical chemical potential μ_* is given by the equation $u_* = U_{ef}(\mu_*)/T$ with the effective potential depth U_{ef} being defined in (A9), and reads

$$\frac{\mu_*}{T} = \ln \frac{e^{|u_*|} - 1}{e^{|U|/T} - e^{|u_*|}}. \quad (\text{A12})$$

Since the contact probability P_b is zero at the unbinding point, the critical sticker concentration is given by

$$X_* = \frac{e^{\mu_*/T}}{a^2(1 + e^{\mu_*/T})} = \frac{e^{|u_*|} - 1}{a^2(e^{|U|/T} - 1)}. \quad (\text{A13})$$

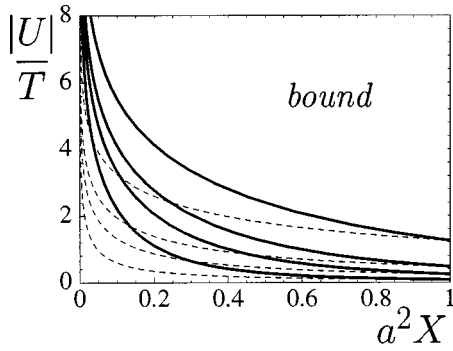


FIG. 12. Dimensionless binding energy U/T as a function of the dimensionless concentration $a^2 X$ of the stickers for continuous unbinding transitions: (thick lines) A pair of two-component membranes with identical sticker concentration X ; and (dashed lines), a single two-component membrane with sticker concentration X in front of a homogeneous substrate. The dimensionless potential range of the stickers is $z_v = 0.1, 0.3, 0.5$, and 1 (bottom to top).

The critical potential depth u_* can be determined by Monte Carlo simulations. From MC data for the contact probability P_b as a function of the potential depth u for several potential ranges z_v , see [13], we find $u_* = -1.25 \pm 0.05$ for $z_v = 0.1$, $u_* = -0.47 \pm 0.03$ for $z_v = 0.3$, $u_* = -0.24 \pm 0.02$ for $z_v = 0.5$, and $u_* = -0.075 \pm 0.010$ for $z_v = 1$. The unbinding lines in the $(a^2 X, |U|/T)$ -plane resulting from (A13) and the above values for u_* are shown in Fig. 12 as dashed lines.

Because of the continuous character of the unbinding transition, there is no lateral phase separation in the multi-component membrane in the absence of attractive cis interactions between the flexible stickers in accordance with Ref. [10]. This is a direct consequence of Eq. (A11) and the continuity of the contact probability P_b .

APPENDIX B: TWO MEMBRANES WITH STICKERS

A. Flexible stickers without cis interactions

The adhesion of a pair of multicomponent membranes can be described by the grand canonical Hamiltonian

$$\mathcal{H}\{l, n, m\} = \mathcal{H}_{el}\{l\} + \sum_i [n_i m_i V(l_i) - n_i \mu_1 - m_i \mu_2] \quad (\text{B1})$$

for flexible stickers in the absence of cis interactions. Here, n and m are the concentration fields of the membrane 1 and 2, respectively, which adopt the values $n_i = 0, 1$ and $m_i = 0, 1$. As in the case of biological membranes, the transinteraction $V(l_i)$ now is mediated by ‘‘lock-and-key’’ pairs of stickers with $n_i = 1$ and $m_i = 1$, which are anchored in the opposing membranes. The molecular adhesion potential $V(l_i)$ will be characterized in the following again by the square-well potential (4) with binding energy $U < 0$ and potential range l_v . The elastic energy of the membranes with uniform bending rigidities κ_1 and κ_2 can be written in the form (2) where κ now is the effective bending rigidity $\kappa_1 \kappa_2 / (\kappa_1 + \kappa_2)$. Finally, the relative chemical potential of the stickers are denoted by μ_1 and μ_2 .

Since the Hamiltonian (B1) is linear in the concentration fields n and m , the partition function can be written as

$$\mathcal{Z} = (1 + e^{\mu_1/T})^N (1 + e^{\mu_2/T})^N \times \left[\prod_i \int_0^\infty dl_i \right] e^{-[\mathcal{H}_{el}\{l\} + \sum_i V_{ef}(l_i)]/T} \quad (\text{B2})$$

after the summation of the sticker degrees of freedom. The effective potential now is

$$V_{ef}(l_i) = -T \ln \frac{1 + e^{\mu_1/T} + e^{\mu_2/T} + e^{(\mu_1 + \mu_2 - U)/T}}{(1 + e^{\mu_1/T})(1 + e^{\mu_2/T})} \times \theta(l_v - l_i) \equiv U_{ef} \theta(l_v - l_i). \quad (\text{B3})$$

The two membranes unbind at a critical value u_* of the reduced effective potential depth $u = U_{ef}/T$, which depends on the rescaled potential range $z_v = (l_v/a)\sqrt{\kappa/T}$, see Appendix A.1. For equal chemical potentials of the stickers, i.e., for $\mu_1 = \mu_2 = \mu$, the critical value μ_* is determined by the equation $u_* = U_{ef}(\mu_*)/T$ and reads:

$$\mu_* = T \ln \frac{e^{|u_*|} - 1 + \sqrt{e^{|U|/T} - 1} \sqrt{e^{|u_*|} - 1}}{e^{|U|/T} - e^{|u_*|}}. \quad (\text{B4})$$

The critical concentration $X_* = (1/a^2)e^{\mu_*/T}/(1 + e^{\mu_*/T})$ at which the membranes unbind then is given by

$$X_* = \frac{1}{a^2} \sqrt{\frac{e^{|u_*|} - 1}{e^{|U|/T} - 1}}. \quad (\text{B5})$$

Unbinding lines in the $(a^2 X, |U|/T)$ plane resulting from Eq. (B5) are displayed in Fig. 12 as solid lines. The dashed lines correspond to the unbinding lines for a single multicomponent membrane adhering to a homogeneous substrate, see Eq. (A13). For this latter geometry, the extent of the bound phases is larger for given rescaled potential range z_v since the stickers bind to any lattice site of the substrate. In contrast, ‘‘lock-and-key’’ stickers of this section can only bind if $n_i = 1$ and $m_i = 1$.

B. Flexible stickers with attractive cis interactions

A general Hamiltonian for stickers with attractive cis interactions has to include quadratic terms in the concentration fields n and m . For simplicity, we consider here only the case of stickers with the same chemical potential $\mu = \mu_1 = \mu_2$ and cis-interaction matrix W_{ij} in the two membranes. This applies in particular to the situation of homophilic binding where the stickers in the opposing membranes are identical. The Hamiltonian then can be written as

$$\mathcal{H}\{l, n, m\} = \mathcal{H}_{el}\{l\} + \sum_i [n_i m_i V(l_i) - \mu(n_i + m_i)] + \sum_{\langle ij \rangle} W_{ij}(n_i n_j + m_i m_j), \quad (\text{B6})$$

with the nearest-neighbor interaction (5). To develop a mean-field theory as in Sec. IV, we use again the variational principle (7), now with

$$\mathcal{H}_o = \mathcal{H}_{el} + \sum_i [n_i m_i V(l_i) + (B - \mu)(n_i + m_i)]. \quad (\text{B7})$$

This leads to the upper boundary $\mathcal{F}_>$ for the free energy:

$$\begin{aligned} \mathcal{F} \leq \mathcal{F}_o - \frac{B}{A} \sum_i [\langle n_i \rangle_o + \langle m_i \rangle_o] + \frac{1}{A} \sum_{\langle ij \rangle} W_{ij} [\langle n_i n_j \rangle_o \\ + \langle m_i m_j \rangle_o] \leq \mathcal{F}_o - \frac{2B}{a^2} \langle n_i \rangle_o + \frac{4W}{a^2} \langle n_i \rangle_o^2 \equiv \mathcal{F}_>. \quad (\text{B8}) \end{aligned}$$

A minimization with respect to the variational parameter B results again in the self-consistency equation

$$B = 4W \langle n_i \rangle_o. \quad (\text{B9})$$

Phase diagrams that were numerically derived from the mean-field Eqs. (B8) and (B9) are displayed in Fig. 11 and compared to the corresponding diagrams for the adhesion of a single two-component membrane to a homogeneous substrate. The phase diagrams for the two geometries differ at small values of the sticker binding energy $|U|$, but agree at large values of $|U|$ where the phase behavior becomes independent of this parameter since the majority of stickers is already bound. For “lock-and-key” stickers, this regime is reached at higher values of $|U|$ since the binding of the stickers is more restricted and requires $n_i = m_i = 1$.

In this appendix, we have considered two-component membranes and flexible stickers, though similar conclusions should also apply to rigid stickers or membranes that additionally contain repulsive molecules. In particular in the regime of high sticker binding energies $|U|$, a similar phase behavior for the two geometries can be expected. Since biological stickers are mostly characterized by high values of the binding energy, this regime is of particular interest.

-
- [1] *Structure and Dynamics of Membranes: Generic and Specific Interactions*, Vol. 1B of *Handbook of Biological Physics*, edited by R. Lipowsky and E. Sackmann (Elsevier, Amsterdam, 1995).
- [2] J. Rädler, T. Feder, H. Strey, and E. Sackmann, *Phys. Rev. E* **51**, 4526 (1995).
- [3] R. Lipowsky, in *Vesicles and Biomembranes*, Vol. 23 of *Encyclopedia of Applied Physics*, edited by G. L. Trigg (VCH Publishers, New York, 1998), p. 199.
- [4] G.I. Bell, *Science* **200**, 618 (1978).
- [5] G.I. Bell, M. Dembo, and P. Bongrand, *Biophys. J.* **45**, 1051 (1984).
- [6] G. I. Bell in *Physical basis of Cell-Cell Adhesion*, edited by P. Bongrand (CRC Press, Boca Raton, FL, 1988), p. 227.
- [7] J. Braun, J.R. Abney, and J.C. Owicki, *Nature (London)* **310**, 316 (1984).
- [8] J. Braun, J.R. Abney, and J.C. Owicki, *Biophys. J.* **52**, 427 (1987).
- [9] R. Bruinsma, M. Goulian, and P. Pincus, *Biophys. J.* **67**, 746 (1994).
- [10] R. Lipowsky, *Phys. Rev. Lett.* **77**, 1652 (1996).
- [11] R. Goetz, G. Gompper, and R. Lipowsky, *Phys. Rev. Lett.* **82**, 221 (1999).
- [12] B. Alberts *et al.*, *Molecular Biology of the Cell*, 3rd ed. (Garland, New York, 1994).
- [13] T. Weikl, R. Netz, and R. Lipowsky, *Phys. Rev. E* **62**, 45 (2000).
- [14] R. Lipowsky, *J. Phys. II* **4**, 1755 (1994); A. Ammann and R. Lipowsky, *J. Phys. II* **6**, 255 (1996).
- [15] R. Bruinsma, A. Behrisch, and E. Sackmann, *Phys. Rev. E* **61**, 4253 (2000).
- [16] S. Komura and D. Andelman, *Eur. Phys. J.* (to be published).
- [17] The temperature T in energy units corresponds to $k_B T'$ where T' is the temperature in Kelvin and k_B denotes Boltzmann's constant.
- [18] R. Lipowsky and S. Leibler, *Phys. Rev. Lett.* **56**, 2541 (1986).
- [19] J.W. Cahn, *J. Chem. Phys.* **66**, 3667 (1977).
- [20] R.R. Netz and P. Pincus, *Phys. Rev. E* **52**, 4114 (1995).
- [21] R.R. Netz, *J. Phys. I* **7**, 833 (1997).
- [22] T. R. Weikl (unpublished).
- [23] E. Evans and D. Needham, *J. Phys. Chem.* **91**, 4219 (1987).
- [24] W. Helfrich, *Z. Naturforsch. A* **A33**, 305 (1978).
- [25] T. R. Weikl, S. Komura, D. Andelman, and R. Lipowsky (unpublished).
- [26] For a table with experimentally determined values for the bending rigidity κ , see U. Seifert and R. Lipowsky, in *Structure and Dynamics of Membranes: From Cells to Vesicles*, Vol. 1A of *Handbook of Biological Physics*, edited by R. Lipowsky and E. Sackmann (Elsevier, Amsterdam, 1995), p. 403.
- [27] P. Bongrand, *Rep. Prog. Phys.* **62**, 921 (1999).
- [28] J. Nardi, T. Feder, R. Bruinsma, and E. Sackmann, *Europhys. Lett.* **37**, 371 (1997).
- [29] A. Albersdörfer, T. Feder, and E. Sackmann, *Biophys. J.* **73**, 245 (1997).
- [30] A. Kloboucek, A. Behrisch, J. Faix, and E. Sackmann, *Biophys. J.* **77**, 2311 (1999).
- [31] D. Braun and P. Fromherz, *Phys. Rev. Lett.* **81(23)**, 5241 (1998).
- [32] D. Gallez and W. Coakley, *Heterog. Chem. Rev.* **3**, 443 (1996).
- [33] R. Merkel *et al.*, *Nature (London)* **397**, 50 (1999).
- [34] U. Seifert, *Phys. Rev. Lett.* **84**, 2750 (2000).
- [35] W. Helfrich, *Z. Naturforsch. C*, **C28**, 693 (1973).
- [36] R. Lipowsky, *Europhys. Lett.* **7**, 255 (1988).